Journal of Power Sources 196 (2011) 10228–10233

Contents lists available at SciVerse ScienceDirect

Journal of Power Sources

journal homepage: www.elsevier.com/locate/jpowsour

Structural, morphological and electrochemical properties of nanocrystalline V_2O_5 thin films deposited by means of radiofrequency magnetron sputtering

I. Quinzeni, S. Ferrari, E. Quartarone*, P. Mustarelli

Department of Chemistry, University of Pavia, Viale Taramelli 12, 27100 Pavia, Italy

ARTICLE INFO

Article history:
Received 5 April 2011
Received in revised form 10 August 2011
Accepted 16 August 2011
Available online 25 August 2011

Keywords:
V_2O_5
Thin films
r.f. magnetron sputtering
Lithium microbattery

ABSTRACT

Due to easiness of preparation and high energy density, V_2O_5 nanocrystalline thin films are particularly attractive as cathode materials for all-solid-state rechargeable lithium microbatteries. However, their electrochemical performances are strictly related to the film microstructure, which, in turn, is related to the nature and parameters of the deposition technique. For this reason, the preparation of thin films with reproducible electrochemical properties is still an open problem.

Here, we report on the deposition of V_2O_5 crystalline thin films by means of reactive radiofrequency (r.f.) magnetron sputtering, using vanadium metal as the target. Different deposition times and substrate temperatures were adopted. X-ray powder diffraction (XRD) and atomic force microscopy were used to investigate the structural and morphological features of the films. In particular, XRD analysis revealed that the deposition parameters affect the crystallographic orientation of the films. A *h* 0 0 orientation is observed in case of thin samples (about 100 nm) prepared at 300 °C, whereas a 1 1 0 preferential growth is obtained for thicker films. Films deposited at 500 °C display a 0 0 1 orientation irrespective on the deposition time.

Reversible Li intercalation/deintercalation processes and high specific capacity are observed for the *h* 0 0-oriented V_2O_5 thinner films, with the *ab* plane arranged perpendicular to the substrate. In this case, the cycling behaviour is very promising, and a stable capacity higher than 300 mAh g^{-1} was delivered in the potential range 3.8–1.5 V at 1*C* rate over at least 70 cycles.

1. Introduction

The development of microdevices is rapidly growing due to the increasing demand for miniaturised systems coming from microelectronics, telecommunication, medical implants field, military industry and Radio Frequency IDentification (RFID) applications. In this context, lithium microbatteries (LMBs) offer important advantages, like light weight, absence of a liquid electrolyte, safety, good environmental compatibility, long life time, and high specific energy. Generally speaking, a lithium microbattery is an all-solid-state system, where cathode, electrolyte and anode are stacked to form a few microns thick cell. Due to the progress in the thin film technology, a great number of systems were proposed in literature during these last years by varying the employed materials [1]. Among the large family of the transition metal-based cathodes, V_2O_5 still seems to be the most interesting one for LMBs, due to its low cost, easiness of preparation and theoretical high energy density. Vanadium pentoxide is characterised by a layered structure in which small alkalyne atoms may be reversibly intercalated and deintercalated. In the particular case of lithium, up to three ions per V_2O_5 unit may be inserted and extracted, so providing an overall capacity of about 440 mAh g^{-1} in the potential range 3.8–1.5 V [2,3]. It can crystallize in several polymorphs, namely the orthorhombic α-V_2O_5 and γ-V_2O_5 phases, the monoclinic or tetragonal β-V_2O_5 and the δ-V_2O_5, that is a modification of the β phase [4], but only the orthorhombic phase is active from an electrochemical point of view. In spite of these positive features, V_2O_5 shows poor structural stability, low conductivity and low intercalation/deintercalation kinetics. In order to overcome such limitations, some improvements were reached by means of two main approaches: (i) the addition of doping transition metals [5]; (ii) the synthesis of nanostructured V_2O_5, in which shorter diffusion paths are available for Li ions [6].

Thin films of V_2O_5 with fairly good electrochemical performances were recently prepared by means of different deposition techniques, including sol–gel process [7,8], spray pyrolysis [9], thermal evaporation [10], electron beam evaporation [11], pulsed laser deposition (PLD) [12,13], chemical vapour deposition [14], ion beam sputtering [15], and d.c. or r.f. sputtering [16–18]. The growth V_2O_5 thin films which good electrochemical properties strictly depends on features like actual oxygen content, thickness and crystallographic phase(s), which in turn are related to the deposition

* Corresponding author. Tel.: +39 0382 987894; fax: +39 0382 987776.
E-mail address: Eliana.Quartarone@unipv.it (E. Quartarone).

0378-7753/$ – see front matter © 2011 Elsevier B.V. All rights reserved.
doi:10.1016/j.jpowsour.2011.08.073

Table 1
Deposition conditions, thickness and rugosity of the V_2O_5 thin films.

Sample	t (h)	T (°C)	Film thickness (nm)	Film rugosity, R_{rms} (nm)
V_2O_5_a	3	300	127	96
V_2O_5_b	3	500	200	126
V_2O_5_c	7	300	320	160
V_2O_5_d	7	500	500	250

technique and to several experimental parameters, like pressure, substrate nature and topology, reactive/non-reactive atmosphere, deposition time, and deposition/annealing temperature. From the point of view of the crystalline structure, it must be stressed that several processes lead to amorphous films, which must be annealed in order to reach the desired orthorhombic phase. However, the annealing step should be avoided because it can cause changes in the V oxidation state and undesired reactions at the substrate interface. Further, V_2O_5 films deposited by different techniques often show different oxide stoichiometries. In addition, high enough specific capacity is delivered only in case of films with thickness not higher than 0.3 μm [18]. Therefore, depending on the employed technique, the optimization of the deposition protocol is a critical task to obtain film with well reproducible electrochemical properties for application as cathodes in LMBs.

Among the wide family of deposition techniques, sputtering processes are the most used due to their versatility, low cost, reasonable deposition rates and simplicity in experimental parameters modulation. Recently, we showed that is possible to modulate the deposition of pure V_2O_3, VO_2 and V_2O_5 from metallic vanadium by properly changing temperature and oxygen partial pressure [19].

In this work we investigated the role of the substrate temperature and film thickness on the crystallographic, microstructural and electrochemical features of α-V_2O_5 thin films, obtained by means of r.f. magnetron sputtering without any post-annealing treatment. By performing cyclic voltammetry and battery tests on a standard lithium cell Li/EC-DEC–$LiPF_6$/V_2O_5, we addressed the influence of degree of crystallinity, preferential growths of the crystallites and film morphology on the Li intercalation/deintercalation processes of the V_2O_5 thin films.

2. Experimental

2.1. Deposition of α-V_2O_5 thin films

Thin films of V_2O_5 were deposited in a high vacuum (10^{-3} Pa) r.f. magnetron sputtering system, which consists of three confocal r.f. sputtering guns at 40–50 mm from the substrate centre. The cathodes are aligned at 30° offset from the substrate normal with an off-axis geometry, in order to minimize the remission effect of the atoms flow. Stainless steel (SS) disks with a diameter of 10 mm (Good Fellow), previously coated by a 150 nm-thick layer of gold as current collector, were chosen as the substrate. The substrate roughness is of 7 nm. Vanadium metal (Good Fellow, 99.999%) was used as the target. The film growth was carried out at a pressure of 1.3 Pa in Ar/O_2 atmosphere (2:1 ratio). The r.f. power was fixed at 100 W for each experiment, whereas two different substrate temperatures (300 °C and 500 °C) were chosen. The film thickness was varied by increasing the deposition time from 3 to 7 h. Deposition rates of about 44 nm h^{-1} and 68 nm h^{-1} were obtained at 300 °C and 500 °C, respectively. Table 1 collects the deposited samples and the sputtering conditions, together with some physical parameters.

2.2. Film characterisation

X-ray diffraction (XRD) patterns were acquired on a Bruker D8 Advance diffractometer equipped with a Cu anode in a q–q geometry. Additional scans in the configuration including a Goebel mirror were also collected.

AFM images (256 × 256 pixels) were obtained with an Auto-Probe CPII microscope (VEECO), operating in contact mod (C-AFM), by means of a pyramidal sharpened silicon tip (curvature radius, <20 nm) on V-shaped cantilevers (resonant frequency, 15 kHz; force constant, 0.03 N m^{-1}) (VEECO). For each analysed film, scans of 8 mm × 8 mm were carried out with a scan rate of 1.0 Hz. A standard 2nd order flattening processing of the images was performed in order to correct the scanner non-linearity. The film thickness was measured by means of a stylus profilometer (KLA Tencor P6 Profiler), equipped with a diamond stylus (radius 2 μm), by applying a force of 2 mg.

The electrochemical tests were performed using a three-electrodes Swagelock-cell where lithium metal was used both as the negative and the reference electrode and a glass-wool (Whatman GF/A) disc was used as the separator. The liquid electrolyte was a standard solution of EC/DEC (1/1 v/v)–$LiPF_6$ (1 M) (Merck). Each cell was assembled in a dry-box under Argon atmosphere (H_2O, O_2 < 1 ppm). The cyclic voltammetry (CV) was performed using an Electrochemical Interface (Solartron 1287) at a scan rate of 0.1 mV s^{-1} in the potential range 2.5–3.8 V. The galvanostatic cycling tests were carried out using an Arbin battery cycler (model BT-2000). The cells were charged and discharged at different rates in the range from 2.5–3.8 V to 1.5–3.8 V. All the cells were tested at room temperature.

3. Results and discussion

3.1. Structural and morphological features of nanocrystalline V_2O_5 thin films

Fig. 1 shows the XRD patterns of the V_2O_5 films of various thicknesses deposited at 300 °C and 500 °C, (see caption). Generally speaking, the main diffraction peaks obtained for every sample are those expected for the orthorhombic V_2O_5 α-phase (JCPDS card n° 41-1426). However, remarkable differences in intensity and number of the diffraction signals are observed depending on the film thickness and deposition temperature. Basically, higher film thickness and substrate temperature lead to more crystalline deposits, as we observe by comparing the plots (a) (V_2O_5_a) and (b) (V_2O_5_b), with the (c) (V_2O_5_c) and (d) (V_2O_5_d) ones, respectively. On the other hand, it is well known from the literature that different deposition temperatures and film thicknesses may induce different crystallographic orientations. In our case, in fact, the thinner sample deposited at 300 °C, shows a h 0 0 preferential growth of the

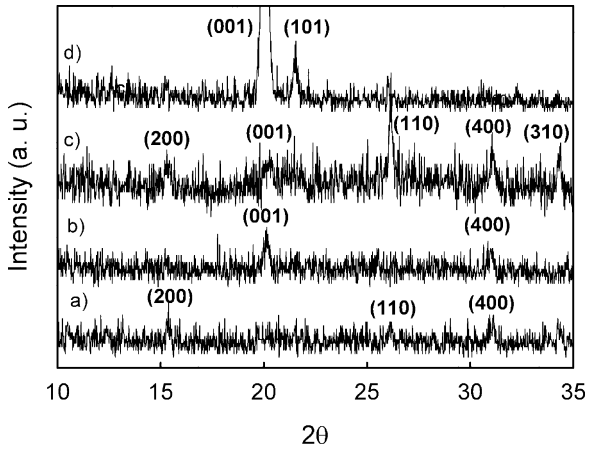

Fig. 1. XRD patterns of V_2O_5 films deposited at different deposition times and temperatures (see Table 1).

Table 2
Lattice parameters, unit cell volume and microstrain ε_{zz} of the deposited V_2O_5 films. The data of V_2O_5_p are taken from the JCPDS card.

Sample	Lattice parameters			Cell volume (Å^3)	ε_{zz}
	a (Å)	b (Å)	c (Å)		
V_2O_5_p	11.498	3.545	4.345	177.10	–
V_2O_5_a	11.423(31)	3.551(9)	4.415(13)	179.12(9)	+1.60
V_2O_5_b	11.397(24)	3.478(7)	4.344(10)	172.23(7)	−0.02
V_2O_5_c	11.464(26)	3.555(7)	4.383(12)	178.67(7)	+0.87
V_2O_5_d	11.464(28)	3.521(28)	4.386(5)	177.09(10)	+0.94

crystallites, with the *ab* planes perpendicularly arranged to the substrate (plot a), in agreement with what already observed in case of V_2O_5 thin films [16,20], However, such a preferential growth is partially lost by increasing the deposition time. In fact, the 1 1 0 direction is favoured in the case of the thicker sample, as demonstrated by the intensity of the signal peaked at 26,14°/2θ (plot 1c). A different situation is found in the case of the films deposited at 500 °C, V_2O_5_b and V_2O_5_d. For both the samples, the predominance of the (0 0 1) peak (at about 20°/2θ) is observed in the XRD patterns. However, only the thicker film is strongly oriented along the *c*-axis with a consequent disposition of the *ab* planes parallel to the substrate.

Table 2 summarises the lattice parameters and the unit cell volumes calculated for each sample. The values of bulk α-V_2O_5 are also reported for the sake of comparison. The unit cell parameters of the films show some differences with respect to the ones of polycrystalline α-V_2O_5. In particular, the *c*-axis length of the oriented samples (V_2O_5_a, V_2O_5_c and V_2O_5_d) is higher than that of bulk, which translates it to a cell volume expansion in the cases of V_2O_5_a and V_2O_5_c, whereas the volume of V_2O_5_d is practically unchanged. In contrast, the V_2O_5_b sample shows a nearly unchanged *c*-axis length and a reduced cell volume (see Table 2). A density of about 3.50 g cm^{-3} is calculated for this last (non-oriented) film deposited at 500 °C, whereas values ranging from 3.34 to 3.38 g cm^{-3} are obtained for the other films.

Greater lattice parameters, and in particular *c*-axis expansions, were reported in the case of V_2O_5 thin films [21] and interpreted in terms of (i) microstrain effects caused by the substrate on the highly anisotropic layered structure of V_2O_5 during its cooling after the deposition [21,22]; or (ii) deviation from the nominal stoichiometry due to the formation of some defective structures [21]. Table 2 reports the values of the film strain along the *c*-axis, ε_{zz}, calculated by the following equation:

$$\varepsilon_{zz} = \frac{c - c_0}{c_0} \times 100$$

where c and c_0 are the lattice parameters of the strained and unstrained V_2O_5, respectively [20,23]. Except for the V_2O_5_b film, which does not show any preferential orientation, positive values of ε_{zz} were found. In the particular case of the films deposited at 300 °C, V_2O_5_a and c, the observed residual strain decreases by increasing the film thickness, in agreement with the literature [20,23]. Concerning the sample V_2O_5_d, whose *c* axis is perpendicular to the substrate, the explanation in terms of microstrain is unlike, and the positive value of ε_{zz} could be attributed to small deviations from the nominal stoichiometry, likely due to the different sticking coefficients of the impinging atomic species at 500 °C with respect to 300 °C. Unfortunately, we are not able to check these stoichiometry variations by means of either XRD data analysis or analytical methods.

The modulation of the sputtering parameters also causes a remarkable change in the film morphology. Fig. 2 shows, as an example, the AFM images obtained in contact mode for the films deposited at 300 °C (part a) and 500 °C (part b), with a thickness of 127 nm and 200 nm, respectively. The images show that both the grains shape and dimension change with the deposition time and the substrate temperature. In particular, a tangled rods-like structure is observed for the sample deposited at 300 °C with crystallite diameters of about 150 nm, whereas grains with a diameter of about 300 nm, arranged in a brick-like texture, are obtained in case of the film deposited at higher temperature. Similar results were reported for V_2O_5 thin films deposited by means of d.c. sputtering with thickness in the range 110–450 nm [16]. Generally speaking, in case of thinner films the crystallites preferentially grow with a rod-like texture [20]. As expected, longer deposition times lead to larger grains. For instance, crystallites with radius higher than 700 nm were found in the thicker sample deposited at 500 °C (not shown). The films deposited at higher substrate temperature and for longer times are characterised by a higher rugosity (see Table 1). This

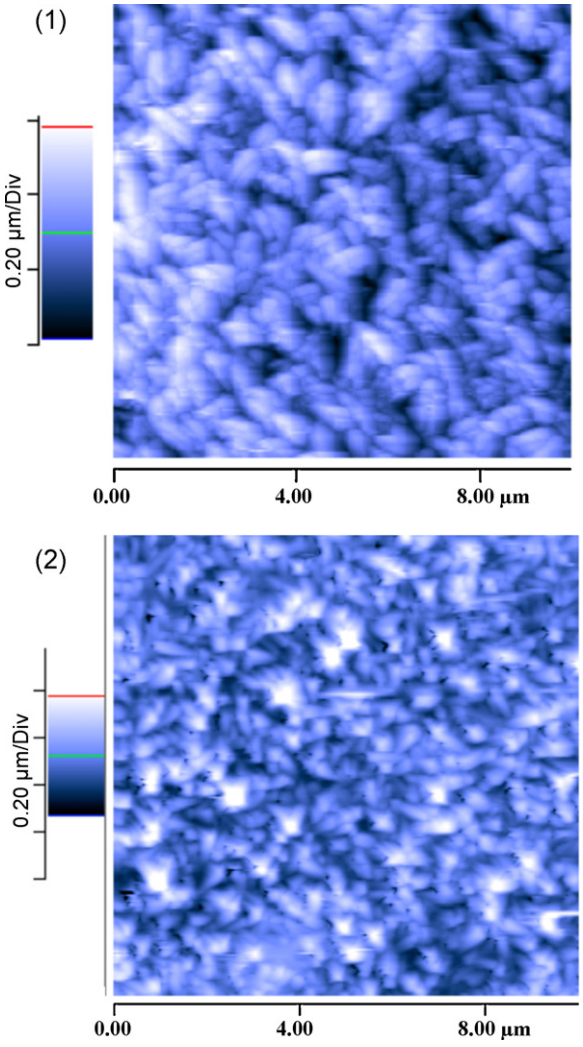

Fig. 2. C-AFM images of two nanocrystalline V_2O_5 thin films: (1) V_2O_5_a and (2) V2O5_b).

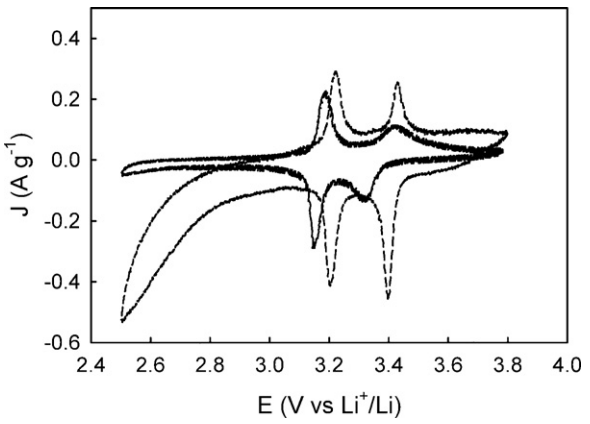

Fig. 3. Cyclic voltammetry sweeps (3rd cycle) in case of the V_2O_5 thin films deposited at 300 °C: V_2O_5_a (dashed line); V_2O_5_c (solid line). Scan rate: 0.1 mV s^{-1}. Liquid electrolyte: EC/DEC (1/1 v/v)–$LiPF_6$ (1 M).

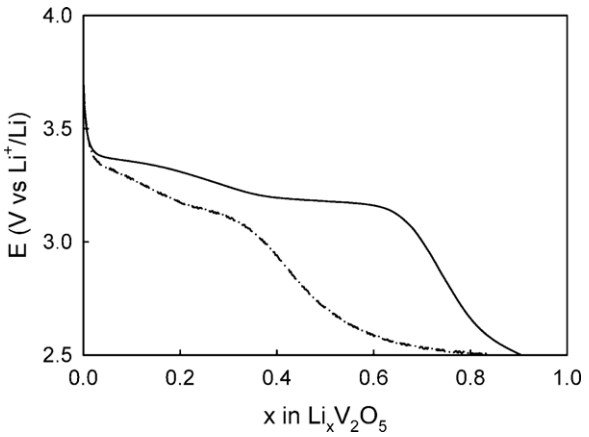

Fig. 5. Discharge profiles in the potential range 3.8–2.5 V in presence of V_2O_5_a (solid line) and V_2O_5_c (dashed dotted line) at 0.2*C* (20th cycle). Liquid electrolyte: EC/DEC (1/1 v/v)–$LiPF_6$ (1 M).

particular behaviour is due to the shadowing mechanism, which dominates the films deposition under the experimental parameters we adopted, leading to a columnar-like growth of the deposit [24]. While we are not able to evaluate the films porosity on the only basis of the AFM images, it is well known that this parameter does decrease by increasing film thickness and/or substrate temperature [24 and references therein].

3.2. Electrochemical investigations

The Li intercalation of V_2O_5 is a complex process, which involves the formation of several $Li_xV_2O_5$ phases depending on the amount of inserted lithium. In the potential range between 2.5 and 3.5 V the insertion process, for instance, leads to the formation of the α-phase $Li_xV_2O_5$ ($x \leq 0.1$), then of the ε-phase $Li_xV_2O_5$ with $0.35 \leq x \leq 0.7$ and of the δ-phase for $x = 1$. For higher Li contents permanent structural changes take place, and the γ and ω-phase ($x = 3$) are obtained [23,25,26]. In order to study the influence of the deposition parameters on the electrochemistry properties of the V_2O_5 thin films, cyclic voltammetry sweeps were firstly performed on all the deposited samples. Figs. 3 and 4 show the CV plots between 2.5 and 3.8 V (vs. Li/Li$^+$) of the samples prepared at 300 °C (V_2O_5_a and c), and 500 °C (V_2O_5_b and d), respectively. Very different cycling behaviours are observed depending on the substrate temperature. For both the samples deposited at 300 °C, the CV profiles are characterised by the typical anodic and cathodic peaks at 3.2 and 3.4 V, which are consistent with a two-steps process. However, the thicker film (V_2O_5_c, solid line) shows less sharp and intense peaks, which are shifted at voltages lower than the expected ones. This effect could be likely related to the microstructure of the film, which was found to be oriented along the (1 1 0) direction, contrary to the thinner film, where a *h* 0 0 preferential growth was observed. Also the higher rugosity of the film (see Table 1), together with the expected lower porosity, can contribute to the worsening of the intercalation/deintercalation process. For what concerns the films deposited at 500 °C, only very weak peaks are observed in the cathodic side, while no signals may be detected in the region of the lithium extraction, thus indicating poor reversibility of the process. Again, this behaviour may be interpreted in terms of different microstructure of the films deposited at different temperatures. In particular, in the case of the films deposited at higher temperature, the lower porosity can become a relevant factor in determining the final electrochemical performances (see following). As already stated, the XRD patterns of the samples prepared at 500 °C show the predominance of the 0 0 1 line, which is the preferential orientation in case of the thicker film. Shortened redox steps at 3.4 V and 3.2 V, and a lower consequent capacity in presence of 0 0 1-oriented deposits with respect to the *h* 0 0 films, were also observed by Navone et al. for films obtained by d.c. sputtering [16]. In that case, the authors stated that in the 0 0 1-oriented films the kinetics of the Li insertion reaction is not so favoured as in case of *h* 0 0-oriented systems, due to a lower porosity, which causes a reduced contact between the active cathodic materials and the electrolyte. We support this conclusion because of the poor performances detected during the charge–discharge experiments carried out on a Li cell based on the V_2O_5_b film (not reported here). On the basis of the cyclic voltammetry results, in the following our attention will be devoted only to the films deposited at 300 °C.

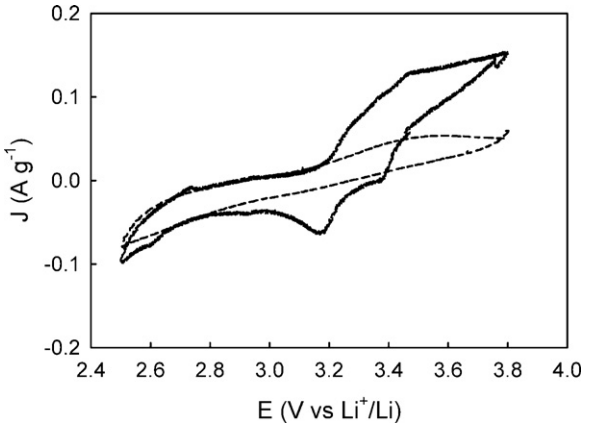

Fig. 4. Cyclic voltammetry sweeps (3rd cycle) of the V_2O_5 thin films deposited at 500 °C: V_2O_5_b (solid line); V_2O_5_d (dashed line). Scan rate: 0.1 mV s^{-1}. Liquid electrolyte: EC/DEC (1/1 v/v)–$LiPF_6$ (1 M).

Fig. 5 compares the discharge profiles of V_2O_5_a (solid line) and V_2O_5_c (dash-dot line) obtained at the 20th cycle at 0.2*C* rate. The two steps of intercalation are still appreciable for both the films. However, different amounts of intercalated lithium are obtained for the two samples. In the case of V_2O_5_a sample, a value of 0.9 Li$^+$ per oxide mole is calculated, in fair agreement with those typically reported for films deposited by r.f. sputtering or other physical deposition techniques [27,28]. In contrast, a slightly lower amount of lithium (0.83) is inserted in the case of the thicker film (V_2O_5_c), which shows different orientation and grains size. A reduced Li insertion again may be related to differences in the microstructure, that influences the kinetic of the diffusion process.

Figs. 6 and 7 report the r.t. charge/discharge behaviours in the potential range 3.8–2.5 V at different current regimes of the

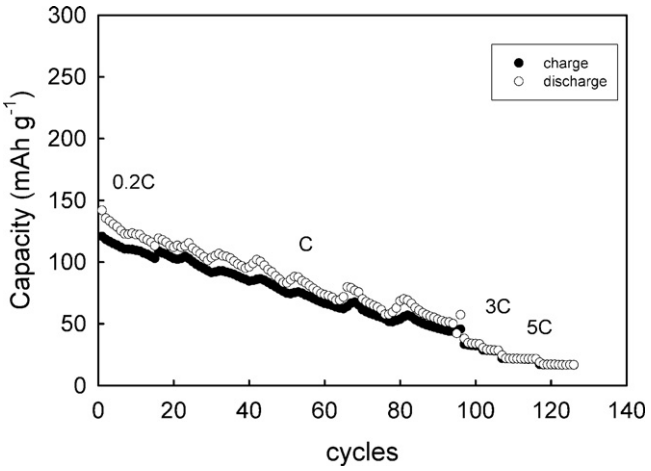

Fig. 6. Cycling behaviour for the V_2O_5_a thin film in the potential range 2.5–3.8 V at different current regimes. Liquid electrolyte: EC/DEC (1/1 v/v)–$LiPF_6$ (1 M).

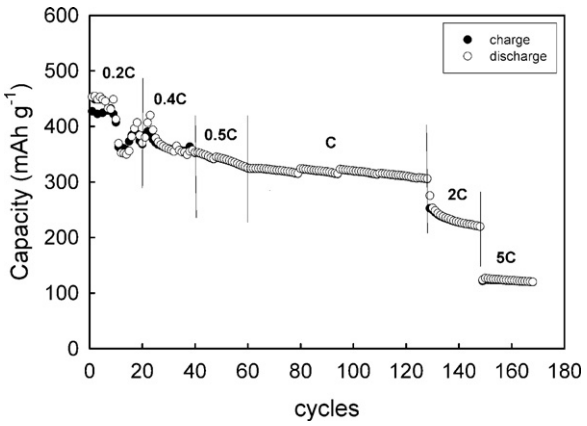

Fig. 8. Cycling behaviour for the V_2O_5_a thin film at different current regimes in the potential range 1.5–3.8 V. Liquid electrolyte: EC/DEC (1/1 v/v)–$LiPF_6$ (1 M).

V_2O_5_a and V_2O_5_c films, respectively. Although the electrochemical history is not exactly the same, a comparison between the performances of the films can be done. At low current regimes (0.2*C*), the delivered specific capacity is about 140 mAh g^{-1} in both cases. This value corresponds to the insertion of one Li ion per formula unit. By increasing the *C* rate, the performances of the V_2O_5_c seem better than those of V_2O_5_a, and a very good plateau is observed for 300 cycles at *C* rate. Moreover, the V_2O_5_c film shows a coulombic efficiency very close to 1, which is higher than that obtained in the case of V2O5_a-based cell, at least up to 2*C* rate. However, the efficiency dramatically falls at 5*C*, when some irreversible processes, such as structural modifications, occur during the insertion/extraction phenomena, contrary to what observed for the thinner cathode. In summary, the thicker film seems preferable in the explored voltage range, which corresponds to the intercalation/deintercalation of one Li^+ per formula unit.

However, technological applications of this material do require to study the electrochemical performances related to the maximum insertion of lithium, i.e. three ions per formula unit. Therefore a discharge up to 1.5 V was carried out for both the samples. The eventual structural changes and the capacity retention of V_2O_5 induced by lithium over-intercalation are indeed important aspects to be considered in the evaluation of the vanadium oxides electrochemical performances, as proved by several studies available in literature (see, for example, Refs. [21,25,28–31]). Fig. 8 shows the room temperature charge-discharge behaviour of the Li/liquid electrolyte/V_2O_5_a cell in the potential range 1.5–3.8 V. At low current regimes, the discharge capacity reaches the maximum value of about 450 mAh g^{-1}, which corresponds to the insertion of three lithium ions per oxide mole. As expected, the delivered specific capacity decreases by increasing the current rate. A good capacity fading of about 3% is obtained at *C* rate over 75 cycles, and values higher than 100 mAh g^{-1} are still retained at 5*C* after 170 cycles. The coulombic efficiency is very close to the unity over all the performed cycles, and no irreversible processes seem to occur, even for the highest current regimes. In contrast, the discharging process up to 1.5 V V_2O_5_c film (not shown here) leads to a severe capacity fading over few cycles. This phenomenon was already observed in the literature, and justified by invoking a slowed Li diffusion in presence of thicker films and irreversible structural modifications in case of films with crystallographic orientations, namely the 1 1 0 one, which seem to be not so favoured from an electrochemical point of view [21,31,32].

Finally, Fig. 9 shows the charge–discharge curves relative to the 4th and 40th cycles of the Li/liquid electrolyte/V2O5_a cell. The profile presents the typical S-shaped form observed also by other authors [21,29], which is related to the formation of the expected ω-$Li_3V_2O_5$ phase.

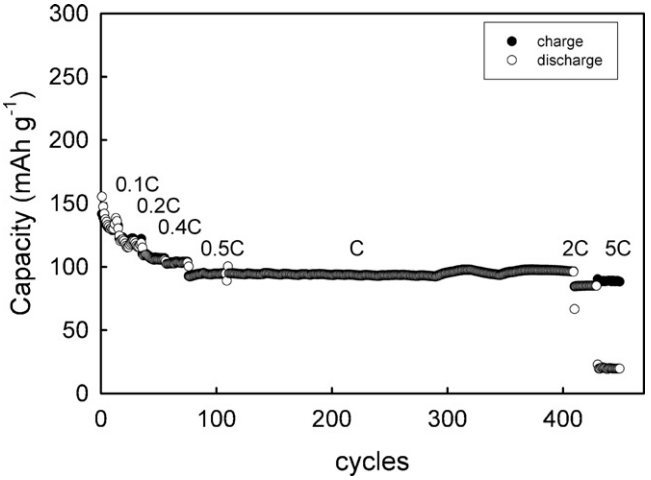

Fig. 7. Cycling behaviour for the V_2O_5_c thin film in the potential range 2.5–3.8 V at different current regimes. Liquid electrolyte: EC/DEC (1/1 v/v)–$LiPF_6$ (1 M).

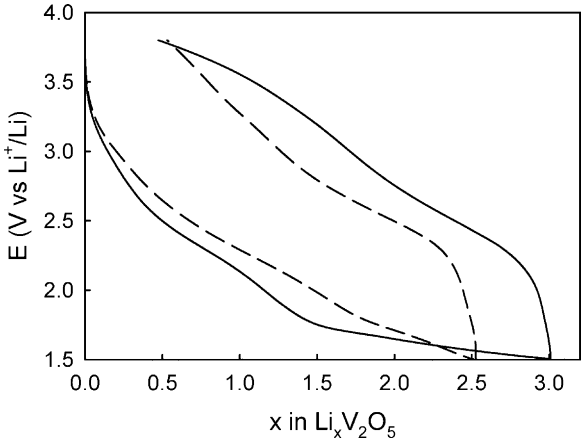

Fig. 9. Discharge profiles at 0.2*C* (solid line) and 0.4*C* (dashed line) relative to the 4th and 40th cycle, respectively, of the cycling process shown in Fig. 8. Liquid electrolyte: EC/DEC (1/1 v/v)–$LiPF_6$ (1 M).

4. Conclusions

Thin films of crystalline V_2O_5 were successfully prepared, without any post-annealing treatment, by means of reactive r.f. magnetron sputtering starting from a vanadium metal target, with different deposition times and substrate temperature. Samples with different crystallographic orientations were obtained by changing the abovementioned parameters. In particular, low film thickness (about 100 nm) and substrate temperature (300 °C) induce a *h*00 preferential growth of the crystallites, with the *ab* planes arranged perpendicular to the substrate. In this case, a rods-like morphology is observed with grain dimensions of about 150 nm. In contrast, a longer deposition time at low substrate temperature leads to 110 orientation, whereas a high substrate temperature leads to 001 orientation, irrespective on the deposition time. From the electrochemical point of view, the *h*00-oriented film shows the best performances in terms of Li intercalation/deintercalation, at least in the case of deep discharge. Specific capacities higher than 300 mAh g^{-1} were obtained in the 3.8–1.5 V potential range, with a capacity fading of 3% at *C* rate over at least 70 cycles. In this case, a coulombic efficiency of about 100% was obtained during the whole cycling test. Therefore, thin V_2O_5 films deposited at low substrate temperature are good candidates as cathodes in lithium microbatteries.

Acknowledgements

The work was funded by FIRB 2006 Project RBIP06AMPP and by Cariplo Project 2010-0506.

References

[1] A. Patil, D.W. Shin, J.-W. Choi, D.-S. Piak, S.-J. Yoon, Mater. Res. Bull. 43 (2008) 1913.
[2] A. Tranchant, R. Messina, J. Perrichon, J. Electroanal. Chem. 113 (1980) 225.
[3] P. Ragupathy, S. Shivakumara, H.N. Vasan, N. Munichandraiah, J. Phys. Chem. C 112 (2008) 16700.
[4] Q. Su, W. Lan, Y.Y. Wang, X.Q. Liu, Appl. Surf. Sci. 255 (2009) 4177.
[5] D.M. Yu, S.T. Zhang, D.W. Liu, X.V. Zhou, S.H. Xie, Q.F. Zhang, Y.Y. Liu, G.Z. Cao, J. Mater. Chem. 20 (2010) 10841.
[6] G. Centi, S. Perathoner, Eur. J. Inorg. Chem. (2009) 3851.
[7] D. Yu, C. Chen, S. Xie, Y. Liu, K. Park, X. Zhou, Q. Zhang, J. Li, G. Cao, Energy Environ. Sci. 4 (2011) 858.
[8] D. Liu, Y. Liu, B.B. Garcia, Q. Zhang, A. Pan, Y.-H. Jeong, G. Cao, J. Mater. Chem. 19 (2009) 8789.
[9] A.A. Akl, J. Phys. Chem. Solids 71 (2010) 223.
[10] X. Wu, F. Lai, L. Lin, Y. Li, L. Lin, Y. Qu, Z. Huang, Appl. Surf. Sci. 255 (2008) 2840.
[11] C.V. Ramana, O.M. Hussain, B. Srinivasulu Naidu, C. Julien, M. Balkanski, Mater. Sci. Eng. B52 (1998) 32.
[12] C.V. Ramana, R.J. Smith, O.M. Hussain, C.C. Chusuei, C.M. Julien, Chem. Mater. 17 (2005) 1213.
[13] R. Teghil, L. D'Alessio, A. De Bonis, A. Galasso, N. Ibris, A.M. Salvi, A. Santagata, P. Villani, J. Phys. Chem. A 113 (2009) 14969.
[14] H. Groult, K. Le Vana, A. Mantoux, L. Perrigaud, P. Doppelt, J. Power Sources 174 (2007) 312.
[15] T. Gallash, T. Stockhoff, D. Baither, G. Schmitz, J. Power Sources 196 (2011) 428.
[16] C. Navone, J.P. Pereira-Ramos, R. Baddour-Hadjean, R. Salot, J. Power Sources 146 (2005) 327.
[17] N. Fateh, G.A. Fontalvo, C. Mitterer, J. Phys. D: Appl. Phys. 40 (2007) 77.
[18] C. Navone, R. Baddour-Hadjean, J.P. Pereira-Ramos, R. Salot, J. Electrochem. Soc. 156 (2009) A763.
[19] Y. Diaz-Fernandez, L. Malavasi, E. Quartarone, J. Mater. Chem. 18 (2008) 5190.
[20] P. Singh, D. Kaur, J. Appl. Phys. 103 (2008) 043507.
[21] C. Navone, R. Baddour-Hadjean, J.P. Pereira-Ramos, R. Salot, J. Electrochem. Soc. 152 (2005) A1790.
[22] D. Habel, O. Gorke, M. Tovar, M. Willinger, M. Ziemann, O. Schwarz, R. Schomacker, H. Schubert, J. Eur. Ceram. Soc. 29 (2009) 1093.
[23] H.C. Ong, A.X.E. Zhu, G.T. Du, Appl. Phys. Lett. 80 (2002) 941.
[24] E. Quartarone, P. Mustarelli, S. Grandi, F. Marabelli, E. Bontempi, J. Vac. Sci. Technol. A: Vac. Surf. Films 25 (2007) 485.
[25] C. Delmas, S. Brethes, M. Menetrier, J. Power Sources 34 (1991) 113.
[26] M.S. Whittingham, Chem. Rev. 104 (2004) 4271.
[27] R. Baddour-Hadjean, C. Navone, J.P. Pereira-Ramos, Electrochim. Acta 54 (2009) 6674.
[28] R. Lindstrom, V. Maurice, H. Groult, L. Perrigaud, S. Zanna, C. Cohen, P. Marcus, Electrochim. Acta 51 (2006) 5001.
[29] C. Delmas, H. Cognac-Auradou, J.M. Cocciantelli, M. Menetrier, J.P. Doumerc, Solid State Ionics 69 (1994) 257.
[30] S.-L. Chou, J.-Z. Wang, J.-Z. Sun, D. Wexler, M. Forsyth, H.-K. Liu, D.R. MacFarlane, S.-X. Dou, Chem. Mater. 20 (2008) 7044.
[31] Y.J. Park, K.S. Ryu, K.M. Kim, N.-G. Park, M.G. Kang, S.H. Chang, Solid State Ionics 154–155 (2002) 229.
[32] N. Kumagai, H. Kitamoto, M. Baba, J. Appl. Electrochem. 28 (1998) 41.